

Author Version of : Ocean Dynamics, vol.72; 2022; 207-222

Time-dependent plume front positioning and its dynamics coupled with seasonal river efflux

G. Seena^{*1,2}, K. R. Muraleedharan¹, C. Revichandran¹, S. Abdul Azeez¹, Sebin John^{1,2,3} & Ravikumar C. Nair¹

¹CSIR-National Institute of Oceanography, Regional Centre-Kochi, Kerala, India.

²Research Scholar, Bharathidasan University, Tiruchirappalli, India.

³India Meteorological Department, New Delhi.

*Email: seenaggopal@gmail.com

Abstract

The time-dependent plume front positioning with respect to different tidal phases and its dynamics coupled with seasonal river efflux on the shelf off Kochi, southwest coast of India, was investigated using Finite Volume Community Ocean Model (FVCOM). This region is linked with a monsoonal estuary, characterised by a mixed semidiurnal tide (1 m) and exhibited features of small and large-scale plumes. The interaction between river efflux and tidal phases modulate plume fronts on the shelf, where the density gradients are fortified or weakened by mixing dynamics. Even though the heavy river efflux in the summer monsoon imparts significant momentum on the shelf, the range of frontal fluctuation was curtailed to 2 km by strong monsoon currents. During the transient phase of the season (fall inter-monsoon), the tidal forcings on plume positioning overwhelm the shelf currents, such that the plume front fluctuates between 5-17 km from the inlet (range increasing to ~12 km). During low tides, the region near the inlets was almost homogenised ($R_d < 1$); while during high tides, the region became more stratified due to the transport of high saline coastal water towards the inlet and also by the decreasing kinetic energy (Richardson number, $R_d > 1$). The location of frontal zones suitable for the propagation of internal waves (Froude number, $F \leq 1$) changes as a result of the competition between river efflux and tide-topography interaction. Strong stratified plume frontal regions with high Brunt Vaisala Frequency (N) could be active zones of internal wave generation when the flow decelerates from supercritical to subcritical during the summer monsoon. The release of accumulated potential energy during the transition from high tide to low tide generate the hydraulic jump. This disturbance in the N_{\max} zone together with $F \leq 1$ condition (supercritical flow changed to subcritical flow) favours the generation and propagation of plume induced internal waves on the shelf. Satellite imageries demonstrate such propagation of plume generated internal waves on the shelf off Kochi.

Keywords: Plume Front, Brunt Vaisala Frequency, Richardson Number, Froude Number, Internal waves, Southwest coast of India.

1. Introduction

Freshwater/estuarine plumes are one of the buoyancy sources of nearshore dynamics. The horizontal and vertical extension of freshwater plumes on the continental shelf create plume fronts, which are influenced by riverine efflux and variations in tidal amplitude and phase. The location of the lift-off point fluctuates with the flood and ebb phases of the tidal cycle (Jay and Smith 1990). The river/estuarine discharges into the shelf float as a lens over the ambient coastal waters and are further transported as buoyancy-driven gravity currents. The relaxation of the gravity currents on the shelf region may radiate internal waves that have amplitudes comparable with that of waves generated from tide-topography interactions (Nash and Moum 2005). The Froude number gives an insight into the front's flow characteristics and predicts the probability of internal wave propagation. The accelerating and decelerating phases of the ebb-tidal current play a crucial role in internal wave generation. The transactional regime with approximately matched river flow and wave velocity generates internal waves (da Silva and Helfrich 2008; Groeskamp et al. 2011). Previous studies (Yankovsky and Chapman 1998) have classified plumes into surface advected and bottom advected plumes, depending on the interaction with bottom topography. These classifications strongly determine the locus and offshore spreading of the plume front. Plumes are characterised by land remnants rich in nutrients, suspended sediments, organic and inorganic carbon, etc., eventually affecting the biogeochemistry of the coastal ocean (J. Dagg et al. 2004). The converging surface plume fronts (Garvine and Monk 1974) are often places of high phytoplankton productivity on continental shelves, since they provide critical feeding and breeding sites for organisms at higher trophic levels (Morgan et al. 2005).

The study region (shelf off Kochi, southwest coast of India, SWCI) is associated with a monsoonal estuary – the Cochin estuary (Vijith et al. 2009), which completely flushes about 42 times in a year (Revichandran et al. 2012). According to Seena et al. (2019), these flushed riverine/estuarine discharges float over the high saline shelf water as a plume (Fig. 1). Garvine (1995) classified buoyant plumes into small and large-scale plumes according to the Kelvin number (K). If $K > 1$, the plume is large-scale and influenced by the earth's rotation such that the plume is twisted towards the right/left of its direction of propagation in the northern/southern hemisphere. If $K < 1$, the plume is small-scale, and the effect of the earth's rotation on its propagation is negligible. The peculiarity of the buoyant plume on the shelf off Kochi is that it exhibits features of small-scale and large-scale plume ($K \leq 1$). During the summer monsoon, the plume fringe twists towards the south under the influence of the SWM currents (Smitha et al. 2008; Jineesh et al. 2015) by nullifying the Coriolis force (small-scale plume). While during the winter monsoon, the plume spreads towards the north (large-scale plume) in prevalence with the coastal currents and Coriolis force (Seena et al. 2019).

During the summer monsoon (June-September), the strong southwest wind blows along the shelf induce coastal upwelling (Smitha et al. 2008), which brings subsurface Arabian sea high saline water mass (36 psu) to the surface. The high river discharge of $1749 \text{ m}^3/\text{s}$ (Fig. 2) during this season lowers the salinity of the inlet waters to <5 psu (Seena et al. 2019). This heavy river discharge together with intense coastal upwelling creates strong stratification (Azeez et al. 2021) on the shelf. The summer monsoon is followed by the fall inter-monsoon (October and November), where the southwest monsoon wind weakens, as does the associated precipitation. Compared to the summer monsoon, the stratification is weakened due to the decreased river efflux ($1312 \text{ m}^3/\text{s}$; salinity <18 psu) and the retreat of coastal upwelling.

Winter monsoon (December-February) is characterised by intermittent rainfall and reversal of coastal currents due to the strengthening of the northeast wind. Due to the decreased river discharge ($219 \text{ m}^3/\text{s}$), the shelf water was modified by the estuarine plume (salinity < 30 psu). Meanwhile, this region is occupied by the low saline Bay of Bengal waters (Prasanna Kumar et al. 2004). Thus, stratification on the shelf is comparatively less due to the presence of an estuarine plume over the low saline Bay of Bengal water. Winter monsoon season is followed by the spring inter monsoon (March-May), where the wind is quiescent, and the river discharge is limited to $121 \text{ m}^3/\text{s}$ owing to the lack of freshwater within the estuary, which further weakens stratification. Thus, the shelf waters off Kochi are influenced by independently varying seasonal features and river discharge. As plume-influenced regions always display elevated nutrient concentrations, they support high biological production throughout the year. The variability of the plume on the shelf can be identified by tracing the plume/plume front propagation and its horizontal/ vertical mixing. Recent studies (Spicer et al. 2021) have revealed that tidal mixing plays a significant role in the mixing mechanism of surface advected plumes. The tidal forcing modulate the plume salinity/density fronts; hence the study governing the impact of tides on plumes, frontal positioning and associated dynamics has societal importance as they elevate nutrient concentration and enhance biological production.

A time-series analysis of the plume propagation is needed to delineate the plume front displacement and its vertical mixing due to tidal interaction. This manuscript details the dynamics of freshwater/estuarine plume fronts on the shelf off Kochi by analysing the time-dependent interaction of the plume front with the mixed semidiurnal tide ($\sim 1\text{m}$) (Fig. 3) and seasonal river efflux. As the shelf off Kochi is influenced by the presence of both freshwater and estuarine plumes, we hypothesis that internal wave generation strongly depends on the degree of stratification and tidal phases. The manuscript presents first-hand data on internal wave generation during the transition from high tide to low tide, which could be applicable to other shelf areas linked with tropical estuaries.

2. Methods

The southwest coast of India extends from 8° N to 13° N in the Arabian Sea and is featured by heavy river discharge and seasonally varying currents along the shelf. The largest estuary associated with this shelf is the Cochin (Kochi) estuary, which extends over a length of 96 km (from Munambam to Alappuzha) and covers an area of 256 km². The two inlets (Fort Kochi, 20 m and Munambam, 7 m) serve as the gateway for annual freshwater discharge of 2.2×10^{10} m³ from seven rivers (Periyar, Chalakkudy, Muvattupuzha, Meenachil, Manimala, Pampa and Achankovil) into the coastal water. This freshwater floats as a plume over the ambient coastal water creating strong density/salinity fronts; the positioning of these plume fronts are modulated by tidal phases. The region is influenced by the summer monsoon (SM), fall inter- monsoon (FIM), winter monsoon (WM) and spring inter-monsoon (SIM) with varying monthly average river discharge of 1749 m³/s, 1312 m³/s, 219 m³/s, 121 m³/s in July, October, December and March respectively (Central water commission data (CWC), 2014). In the present study, we analysed the plume protrusion out of the Fort Kochi inlet and its dependence on tidal forcing. The interaction of the plume with the tide and topography along the SWCI was simulated using the Finite Volume Community Ocean Model (FVCOM, v.4.1) with a hydrostatic approximation for the year 2014. FVCOM is an unstructured grid, finite-volume, free surface, three-dimensional primitive equation coastal ocean model that solves the momentum, continuity, temperature, salinity and density equations (Chen et al. 2003). The spatial resolution of the model was assorted from 20 m within 10 km area of the inlet to 50 km towards the open ocean and featured 60,000 elements with 21 vertical sigma levels. A global self-consistent, hierarchical high-resolution geography database available at <http://www.soest.hawaii.edu/wessel/gshhg/> was utilised to delineate land-water interface, while estuaries and backwaters were incorporated by digitising LISS-III data. European Center for Medium Weather Forecast (ECMWF) data was used for surface meteorological forcings, while tidal elevation data was generated from FES 2014 and forced from the open boundary. The river discharge data from CWC (Fig. 2) was used to force the model at the river inlet region, and the open boundary was forced (temperature, salinity and currents) from the global Hycom model (<http://tds.hycom.org/thredds/catalog.html>). The suitable timestep for the model was 1s, and the outputs were recorded every hour. The calibrations and validations of the model were detailed by Seena et al. (2019). At the same time, the model output was compared with *in-situ* salinity observations during the summer and fall inter monsoon of the year 2014 (Fig. 4), and showed good concordance in the vertical and horizontal distribution. The validated model results (24-hour data collected on the 15th day of every month) were used to study the plume front dynamics and its fluctuation with respect to tides and coastal processes off Kochi. Plume induced offshore radiating internal wave propagation off

Kochi was identified from MAXAR technologies (<https://www.maxar.com>) satellite imagery on 30/08/2015. This image was georeferenced using QGIS software and further enhanced by SNAP software.

2.1. Computation

In stratified water columns (plume influenced regions), quantification of stability parameters gives an insight into convection processes. Hesselberg defined the stability of the water column as

$$E = -\frac{1}{\rho} \left\{ \frac{\partial \rho}{\partial S} \frac{\partial S}{\partial z} + \frac{\partial \rho}{\partial T} \left(\frac{\partial T}{\partial z} + \Gamma \right) \right\}$$

Where ρ, S, T are the density, salinity and temperature of the water parcel (plume), z is the depth, T is the adiabatic temperature gradient, and Γ is the isentropic lapse rate of the parcel. On approximation, E can be written as

$$E = -\frac{1}{\rho} \frac{\partial \rho}{\partial z}$$

The “Brunt Vaisala Frequency (N)” in a stratified medium is given by,

$$N = \sqrt{gE} \text{ rad}$$

where g is the acceleration due to gravity.

Bulk Richardson number is the ratio of the potential energy (PE) to the kinetic energy (KE) and is a useful tool for parameterising the mixing process and can be written as

$$R_d = \frac{\Delta \rho g d}{\rho u^2}$$

Where $\Delta \rho$ is the difference in density between the adjacent layers, d is the depth of the water column, ρ the density, and u is the mean velocity of each layer.

The possibility of internal wave propagation in the plume fronts was identified by calculating the Froude number (Kilcher and Nash 2010) as

$$F = \frac{U}{C}$$

Where U is the plume front velocity, and C is the internal wave speed in the medium in which the wave advances.

$$C = \sqrt{\frac{g' h (d - h)}{d}}$$

$$g' = g \frac{\Delta\rho}{\rho_0}$$

Where h is the plume height, d is the depth of the water column and ρ_0 is the maximum density of the water column.

When $F \leq 1$, the supercritical flow becomes subcritical and sets the criterion for internal wave propagation (Nash and Moum 2005).

3. Results

The study region experiences four seasons with considerable variation in the river efflux, which peak in the SM and drop to a minimum in the SIM. Seena et al. (2019) revealed that the plume behaviour varies from freshwater plume to estuarine plume with the seasonal variations in river discharge, which fortifies or weakens the gradients in the frontal zones.

3.1 Plume front positioning with respect to the tidal oscillation

The study region was characterised by a mixed semidiurnal tide (Fig. 3), which played a significant role in modulating the plume front. The plume front positioning with respect to the tides (Fig. 5) reckons the distance travelled by the front in each tidal phase. In the SM, during LLT (Lowest Low Tide), the front (18 psu) occurred at a distance of ~10 km from the inlet, which further extended up to 12 km in HHT (Highest High Tide), again decreased to 10 km in HLT (Highest Low Tide) then increased to 12 km in LHT (Lowest High Tide). The signature of the frontal zone (30 psu) in the FIM was noted at <6 km at HLT and extended to 12 km in LHT. During LLT, the front was discernible at 15 km from the inlet, and during LHT, it prolonged to 17 km. In the WM, the freshwater efflux was reduced, and the front was identified by the 34 psu contour whose offshore extension corresponding to HHT, LLT, LHT, and HLT was 12 km, 9 km, 15 km and 13 km, respectively. The SIM is the region's dry season with comparatively low river efflux where the front (34 psu) extended up to 8 km during LHT and was confined to 5 km during HLT.

3.2 Seasonal variability of plume front characteristics

3.2.1 Summer monsoon

During the SM, the river efflux of 1749 m³/s reached the shelf and formed a freshwater plume over the ambient shelf water. During the LLT, the front touched the bottom up to a distance of 1 km from the inlet; beyond which, the frontal zone detached and extended offshore up to 10 km (Fig. 6). The Brunt Vaisala Frequency maximum (N_{\max}) zone having frequency $>0.3 \text{ s}^{-1}$ was observed between 5–10 km from the inlet, in respect to the stability of the water column. During this period, R_d is <1 , implying

mixing near the inlets, and it was >1 towards the offshore region. Also, the variation in front velocity with wave velocity was well depicted in the F values. During the HHT, the plume floated as a thin lens over the shelf water and had a thickness of ~ 1 m while the offshore extension was more than during the LLT. With respect to the plume spreading, the pattern of N changed in such a way that the N_{\max} zone extended horizontally (~ 9 km) along the surface. R_d was >1 throughout the plume spread region, and the probability for internal wave propagation was higher. After 6 hours from HHT, the plume was influenced by HLT (Fig. 7), where the front touched the bottom up to a distance of 0.5 km, further detached from the bottom and extended ~ 10 km offshore from the inlet. The N_{\max} zone occurred near the surface, but its spreading was limited to about 2 km. The strong outward flow (maximum KE) observed in the inlet region overcame the buoyancy (PE), which was well depicted in the R_d values. Away from the inlet, the flow velocity decreased abruptly and eventually resulted in an area having $R_d > 1$. The $F < 1$ condition was limited only to a small area in the front. Due to the effect of LHT, the front further detached from the bottom, which resulted in the increased offshore extension as a thin layer over the shelf (~ 12 km) water. The pattern of N_{\max} zone, R_d and F was altered respect to the front spreading, which was much similar to that in the HHT.

3.2.2. Fall inter-monsoon

The FIM was characterised by decreased monthly average river discharge of about $1312 \text{ m}^3/\text{s}$; accordingly, we considered the 30 psu contour (estuarine plume) to delineate the plume front. During the HLT (Fig. 8), even though the outward tidal flow was active, the front did not touch the bottom, and it spread only up to a distance of 5 km from the inlet. The N_{\max} existed only within a small area where the R_d was >1 . The F values revealed that the chances of internal wave propagation were limited under these conditions. After 6 hours, the plume was modulated by LHT so that its thickness remained the same as during the HLT, but the offshore extension increased up to 13 km due to enhanced offshore directed pressure gradient. The pattern for N_{\max} and R_d changed according to the plume spreading, while the lower values of $F (<1)$ implied the possibility of wave generation in the frontal zones. Further, the plume was affected by LLT (Fig. 9), during which the front touched the bottom for a few kilometres (<1 km) and detached subsequently. Due to the strong pulling in the LLT, the offshore extension of the plume increased to 15 km. The spreading of the N_{\max} zone was increased throughout the frontal zone where R_d was always >1 , but the possibility for internal wave propagation was limited to the inlet only. The influence of the HHT on the plume made it a very thin lens over the ambient shelf water with an offshore extension of 17 km and a uniform thickness of <1 m. Even though the FIM was featured by considerable river discharge, the mixing of the plume was less due to weak winds, such that the plume floated as a thin lens over the shelf waters. The N_{\max} zone maintained a similar spatial

extension as that of the plume with $R_d > 1$. A smaller value of $F < 1$ was noticed in the surface layers near the inlet, with a limited area of spreading.

3.2.3. Winter monsoon

The WM is the next season, during which the river efflux to $219 \text{ m}^3/\text{s}$. The shelf lacks freshwater efflux, so we consider the 34 psu contour to identify the estuarine plume influenced area or to demarcate the plume front. During the HHT (Fig. 10), the front extended up to a distance of 12 km and floated as a thin layer over the ambient shelf water. The maximum frequency in the N_{max} zone was about 0.2 s^{-1} . Buoyancy energy and the R_d exhibited a similar pattern to that of the plume, but the $F < 1$ condition was satisfied only in restricted regions of the front. During the LLT, the plume touched the bottom up to a distance of 1 km from the inlet; beyond this, it detached and extended up to 9 km offshore. The N_{max} zone was very thin, and R_d varied with the energy of the plume, while the $F < 1$ condition existed below the considered frontal zone. Further, the plume was acted upon by LHT (Fig. 11) such that the front detached from the bottom and extended horizontally to 15 km. The N_{max} zone was observed as a thin film on the shelf region, but due to the reduced flow velocity, the $R_d > 1$ condition was satisfied by a broad area in the plume-influenced zone. The probability of internal wave propagation was more within 5 km of the inlet. After 6 hours, the plume was modified by HLT so that both the horizontal extension of the plume (13 km) and the N_{max} zone were reduced. The pattern of R_d and F was similar to that during LHT.

3.2.4. Spring inter-monsoon

SIM is the dry phase of the season, where the monthly average river efflux into the estuary was reduced to $121 \text{ m}^3/\text{s}$. The salinity of the plume increased due to the scanty river efflux, and hence the 34 psu contour was used to delineate the plume front. During the LLT (Fig. 12), the front neither touched the bottom nor extended beyond 6 km from the inlet. The maximum possible value for N within this 6 km was less (0.1 s^{-1}). Due to the reduction in PE, the area having $R_d > 1$ was negligibly small on the shelf region. The F values that the criteria for internal wave propagation were not satisfied during the LLT phase. Further, the plume was amended by the LHT (Fig. 13) into a thin layer over the inshore waters. Due to the upward pushing of tides, the offshore spreading of the plume increased to 8 km. The N value was increased to 0.25 s^{-1} , and the spatial area of the plume having $R_d > 1$ was extended. During the HLT, the plume extension was reduced to $< 6 \text{ km}$; concurrently, N and R_d were also modified. Due to the negligible density gradients in the water column, the possibility of internal wave propagation in the frontal region was insignificant. After 6 hours, the plume was influenced by the HHT (Fig. 12); its thickness near the inlet reduced to 1 m from 7 m (HLT), and the offshore spreading increased to 7 km

from 5 km. Even though the frontal zone satisfied the condition of internal wave propagation, the frequency of oscillation of the water column was significantly reduced.

4. Discussion

The plume front is the narrow region on the shelf where the physical properties change abruptly, forming a boundary between the outward flowing buoyant water over the ambient coastal water (Garvine and Monk 1974). As fronts serve as the biological hotspots, it is imperative to understand the offshore limit of plume fronts due to tide-topography interactions. The study by (Wei et al. 2017) revealed that tidal perturbation plays a significant role in the modulation and detachment of the plume. This paper details the dynamics of tidally modulating freshwater/estuarine plume fronts on the shelf off Kochi and the possible conditions for internal wave propagation.

4.1. Factors influencing plume front positioning and seasonal variability in characteristics

During SM, the plume fronts along the SWCI are influenced by heavy river discharge, intense coastal upwelling, strong southerly coastal current, and tidal phases. It was expected that the offshore extension of the plume should be highest, but it was limited to 10-12 km (Fig. 5) due to strong southward moving coastal currents (Jineesh et al. 2015). The variation in plume front positioning over the shelf with respect to tidal phases is minimum (~2 km only) during this season.

During the low tide, enhanced efflux from the estuary caused the front to touch the bottom (the lift-off point is about 1 km from the inlet). In contrast, the subsequent high tide uplifted the front from the bottom and extended it offshore (Fig. 6 and Fig. 7). The time-series data revealed that the flood currents were not adequate to increase the salinity of the estuary > 18 psu due to the heavy river efflux. The protrusion of this modified low saline water (18 psu) over the ambient shelf water serves as an “estuary at sea” in the monsoon season. The N_{\max} zone always lies away from the inlet because the vertical gradients were maximum at a certain distance from the inlet. High stratification was noticed on the shelf due to the protrusion of freshwater plumes over the upwelled water (Smitha 2005). In low tide, the water column near the inlets was homogenised (mixed) due to increased KE ($R_d < 1$). But, a short distance from the inlet, the plume velocity decreased and was not adequate to homogenise the water column ($R_d > 1$). During the high tide, high saline upwelled water intrude towards the inlet (Martin et al. 2010), while the plume extends offshore as a lens of low saline water. The water column was more stratified under this condition with more significant PE, which was well reflected in the high R_d values. The N_{\max} zone always exists near to the surface (< 2.5 m), while $F \leq 1$ condition (water column thickness ranging from 1 m in the offshore region to 7.7 m in the inlet) varies with tidal phases. During the high tide phase, freshwater outflow from the Cochin estuary is only through surface layers, while

bottom layers showed an inward flow of high saline upwelled waters. The plume potential energy trapped during the high tide (Fig. 14) was released during the transitional phase, where the supercritical flow changed to subcritical $F \leq 1$. This satisfies the condition for the generation of internal waves. Satellite imageries (Fig. 15) and propagation of potential energy packets confirm the existence of plume generated internal waves on the shelf off Kochi.

The freshwater efflux into the estuary declined in the FIM season. The positioning of the front (~17 km during the HHT and ~5 km in HLT) was mainly controlled by the tidal phases (Fig. 5) due to the weakening of coastal currents. The range of frontal fluctuation was about 12 km, which was much more than the SM (2 km). Except for the LLT, the plume floated as a lens over the shelf water throughout all the tidal phases (Fig. 8 and Fig. 9). The N_{\max} zone was always near the surface, and maximum spreading during the HHT was driven by the enhanced offshore-directed pressure gradient. Even though the extension of the N_{\max} zone was higher, the condition for internal wave propagation was satisfied within a limited zone (<5 km). The reduced river discharge decreased the accumulation of potential energy during the high tide, which was insufficient to generate a hydraulic jump near the flow transition zone.

In the WM, the northward-flowing currents controlled the dynamics of the shelf region, and hence the plume fringe twisted towards the north (Seena et al. 2019). The range of frontal fluctuation was about 6 km (Fig. 5), which was lesser than the FIM, and this was mainly due to the declined river efflux. Even though the horizontal and vertical extension of the plume was maximum in the LHT (Fig. 11), the N_{\max} zone was very thin, close to the surface. Throughout all the tidal phases (Fig. 10 and Fig. 11), condition $F \leq 1$ was satisfied up to a distance of <5 km from the inlet, but the reduced stratifications were not enough to generate internal waves. Due to the reduced river efflux in the SIM, the tidal dynamics play a significant role in determining shelf kinetic energy than the buoyancy force (Fig. 12 and Fig. 13). Stratification was mainly driven by warming due to high solar insolation; thus, N_{\max} zone was insignificant during this season. Thus, the possibility of plume generated internal wave is the least during SIM.

4.2. The mechanism of plume generated internal waves

Heavy river discharge during the monsoon months (Revichandran et al., 2012) contributed to large outflow through the Fort Kochi inlet, which was modulated by the tidal phases. During the high tide phase, freshwater outflow from the estuary occurs only through surface layers, while bottom layers showed an inward flow of high saline upwelled water. Due to this, potential energy (Fig. 14) is accumulated in the inlet region which release as a hydraulic jump during the transitional tidal (high

tide to low tide) phase. Existence of the N_{\max} zone together with $F \leq 1$ condition (supercritical flow changed to subcritical flow) favours the generation and propagation of plume induced internal waves on the shelf. Satellite imageries (Fig. 15) corroborate the existence of internal waves on the shelf off Kochi.

5. Conclusion

The manuscript details the dynamics of the time-dependent buoyant outflow with respect to the seasons and different tidal phases on the shelf off Kochi, SWCI. The interaction of the seasonal river efflux with the mixed semidiurnal tide creates plume fronts (frontogenesis) on the shelf whose gradients are fortified or weakened by mixing dynamics. After coming out of the inlet (Fort Kochi inlet), the plume floats over the shelf water throughout all the tidal phases except at low tides, in which the plume touched the bottom up to a certain distance (<1 km) from the inlet, thereby exhibit the features of the surface advected plume. During the SM, the offshore extension of the plume front was initially driven by the quantity and momentum of freshwater efflux and tidal currents; and it was reduced (range of fluctuation was ~ 2 km) by the prevailing strong SWM currents. In contrast, in the transient phase (FIM) of the season, tidal forcings and the plume energy overwhelmed the shelf dynamics/currents and played a significant role in frontal positioning (range of frontal fluctuation was ~ 12 km). The range of plume front fluctuation with respect to tidal phases was about 6 km and 3 km during WM and SIM, respectively. Even though the heavy river efflux during SM induced strong stratification on the shelf waters, the condition for the propagation of internal waves was satisfied only when the front velocity decelerated from supercritical to subcritical. An accumulation of potential energy near the inlet during the high tide and its subsequent release during the transitional phase generates the hydraulic jump. This perturbation, in a region that satisfies the $F \leq 1$ condition and is characterised by strong stratification, leads to the propagation of internal waves. Satellite imageries confirm such propagation of plume generated internal waves on the shelf off Kochi.

Acknowledgements

The Department of Science and Technology funded the study under the WOS-A scheme (GAP 2908), and the first author is very thankful to DST. The authors are grateful to the Director, CSIR-NIO and SIC, NIO-RC Kochi, to fulfil the studies. A special acknowledgement to the FVCOM development team members in The Marine Ecosystem Dynamics and Modeling Laboratory, UMASSD, for providing the FVCOM source code. We sincerely acknowledge Dr Usha V. Parameswaran, a native English speaker and project scientist at CMLRE, Ernakulam, for proof editing of the manuscript.

Author Contributions

Seena, G., (G.S.), Muraleedharan, K.R., (K.R.M.), Revichandran, C., (C.R.), Abdul Azeez, S., (S.A.A.), Sebin John, (J.S.) and Ravikumar C. Nair, (R.C.N.); G.S. managed the funding, data analysis and writing of the manuscript; K.R.M. conceived the problem, field survey, analysis and interpretation of the data; C.R. oversaw the project, was involved in the discussion and draft preparation; K.R.M., S.A.A., G.S., J.S., and R.C.N., were involved in the modelling studies; G.S., S.A.A., and R.C.N., prepared the figures and model validation diagrams. All authors reviewed the manuscript.

Declarations

Ethical statement: This article does not contain any studies with human participants or animals performed by any of the authors

Consent statement: For this type of study formal consent is not required.

Conflict of Interest: The authors declare no competing interests.

Data availability statement

The data that support the findings of the study are available from the corresponding author, Seena G., upon reasonable request.

The data utilised for land water-interface and bathymetry (GEBCO) were available online at <http://www.soest.hawaii.edu/wessel/gshhg/> and at (<https://download.gebco.net/>) respectively. Model forcings can be obtained from ECMWF (<https://apps.ecmwf.int/datasets/data/interim-full-daily/levtype=sfc/>). The open boundary inputs were accessible from global Hycom model (<http://tds.hycom.org/thredds/catalog.html>). Model data will be available upon request to the corresponding author, and the in-situ data used for model validation will be available upon request to CSIR-NIO data repository (www.nio.org).

References

- Azeez A, Revichandran C, John S, et al (2021) Sound speed variation in the coastal waters off Cochin and signature of subsurface maxima. *Ocean Dyn* 71:923–933
- Chen C, Liu H, Beardsley RC (2003) An unstructured grid, finite-volume, three-dimensional, primitive equations ocean model: application to coastal ocean and estuaries. *J Atmos Ocean Technol* 20:159–186
- da Silva JCB, Helfrich KR (2008) Synthetic Aperture Radar observations of resonantly generated internal solitary waves at Race Point Channel (Cape Cod). *J Geophys Res Ocean* 113
- Garvine RW (1995) A dynamical system for classifying buoyant coastal discharges. *Cont Shelf Res* 15:1585–1596

- Garvine RW, Monk JD (1974) Frontal structure of a river plume. *J Geophys Res* 79:2251–2259
- Groeskamp S, Nauw JJ, Maas LRM (2011) Observations of estuarine circulation and solitary internal waves in a highly energetic tidal channel. *Ocean Dyn* 61:1767–1782
- J. Dagg M, Benner R, Lohrenz S, Lawrence D (2004) Transformation of dissolved and particulate materials on continental shelves influenced by large rivers: Plume processes. *Cont Shelf Res* 24:833–858. <https://doi.org/10.1016/j.csr.2004.02.003>
- Jay DA, Smith JD (1990) Residual circulation in shallow estuaries: 1. Highly stratified, narrow estuaries. *J Geophys Res Ocean* 95:711–731
- Jineesh VK, Muraleedharan KR, John KL, et al (2015) Mesoscale process-induced variation of the West India Coastal Current during the winter monsoon. *Environ Monit Assess* 187:1–13
- Kilcher LF, Nash JD (2010) Structure and dynamics of the Columbia River tidal plume front. *J Geophys Res Ocean* 115
- Martin GD, Muraleedharan KR, Vijay JG, et al (2010) Formation of anoxia and denitrification in the bottom waters of a tropical estuary, southwest coast of India. *Biogeosciences Discuss* 7:1751–1782
- Morgan CA, De Robertis A, Zabel RW (2005) Columbia River plume fronts. I. Hydrography, zooplankton distribution, and community composition. *Mar Ecol Prog Ser* 299:19–31
- Nash J, Moum JN (2005) River plumes as a source of large-amplitude internal waves in the coastal ocean. *Nature* 437:400–403
- Prasanna Kumar S, Narvekar J, Kumar A, et al (2004) Intrusion of the Bay of Bengal water into the Arabian Sea during winter monsoon and associated chemical and biological response. *Geophys Res Lett* 31
- Revichandran C, Srinivas K, Muraleedharan KR, et al (2012) Environmental set-up and tidal propagation in a tropical estuary with dual connection to the sea (SW Coast of India). *Environ Earth Sci - Env EARTH SCI* 66:. <https://doi.org/10.1007/s12665-011-1309-0>
- Seena G, Muraleedharan KR, Revichandran C, et al (2019) Seasonal spreading and transport of buoyant plumes in the shelf off Kochi, South west coast of India-A modeling approach. *Sci Rep* 9:1–15
- Smitha BR, Sanjeevan VN, Vimalkumar KG, Revichandran C (2008) On the Upwelling off the Southern Tip and along the West Coast of India. *J Coast Res* 95–102. <https://doi.org/10.2112/06-0779.1>
- Spicer P, Cole KL, Huguenard K, et al (2021) The Effect of Bottom-Generated Tidal Mixing on Tidally Pulsed River Plumes. *J Phys Oceanogr* 51:2223–2241
- Vijith V, Sundar D, Shetye SR (2009) Time-dependence of salinity in monsoonal estuaries. *Estuar Coast Shelf Sci* 85:601–608
- Wei Q, Yu Z, Wang B, et al (2017) Offshore detachment of the Changjiang River plume and its ecological impacts in summer. *J Oceanogr* 73:277–294

Yankovsky AE, Chapman DC (1998) A simple theory for the fate of buoyant coastal discharges. Oceanogr Lit Rev 3:435

Figures

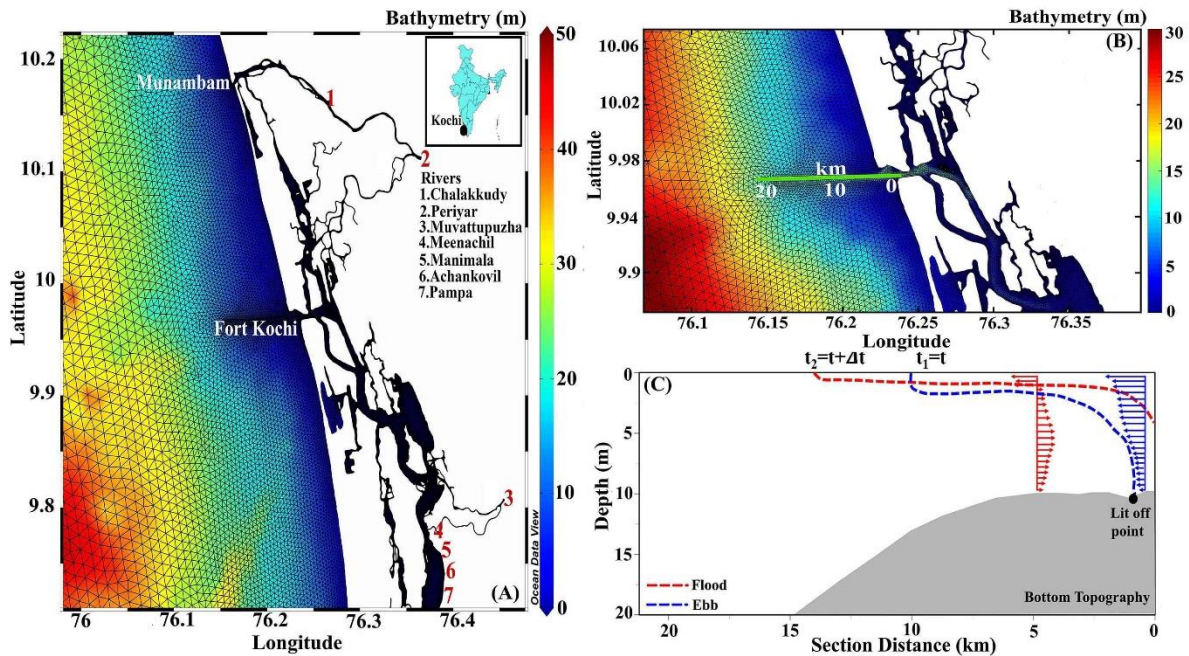


Figure 1. The geographical area (upper panel) of SWCI articulating finite elemental grid for the FVCOM study. The interaction of the front during the flood and ebb phase of the tide with bottom topography is detailed in the lower panel.

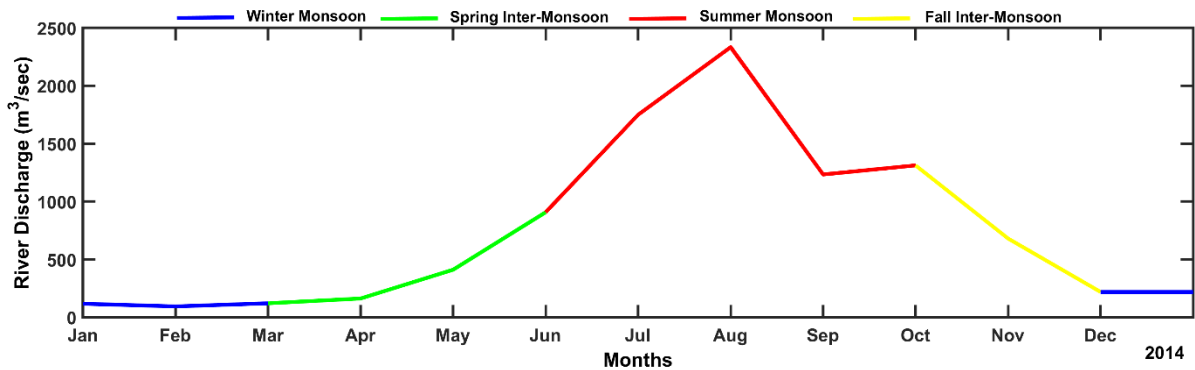


Figure 2. The monthly averaged river discharge data from the seven rivers into the Cochin estuary

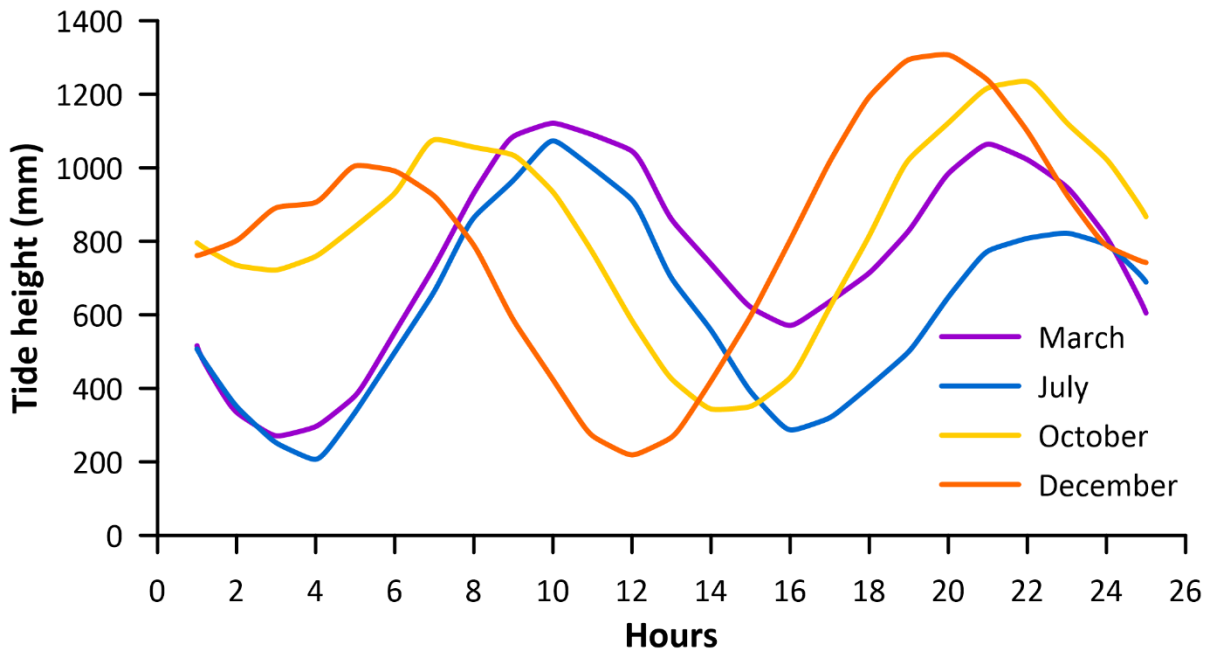


Figure 3. The seasonal tidal variations (mixed semidiurnal) observed on the shelf off Kochi in the year 2014.

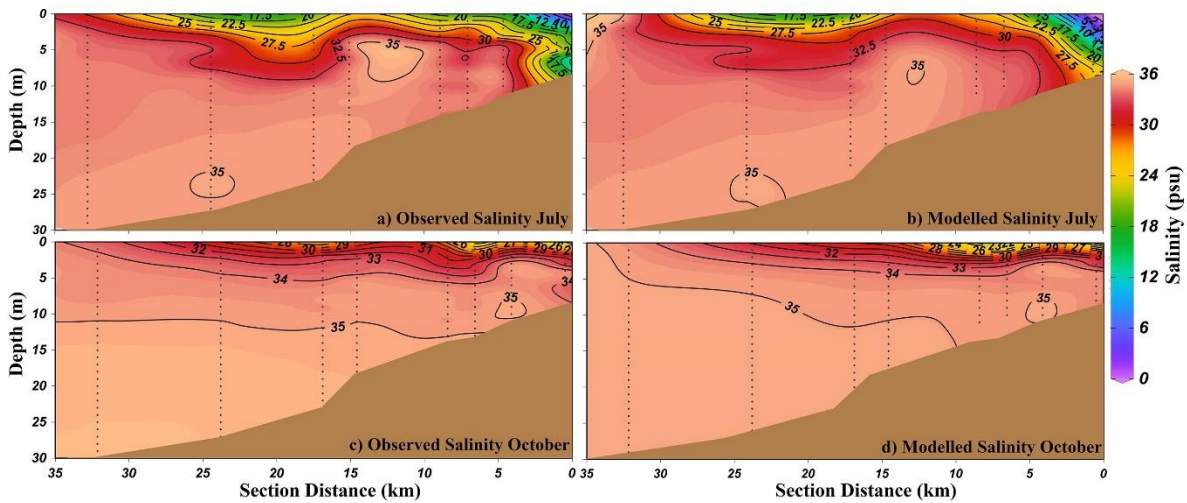


Figure 4. The vertical salinity validation of model data with *in-situ* data in the Fort Kochi inlet during the summer monsoon and fall inter-monsoon.

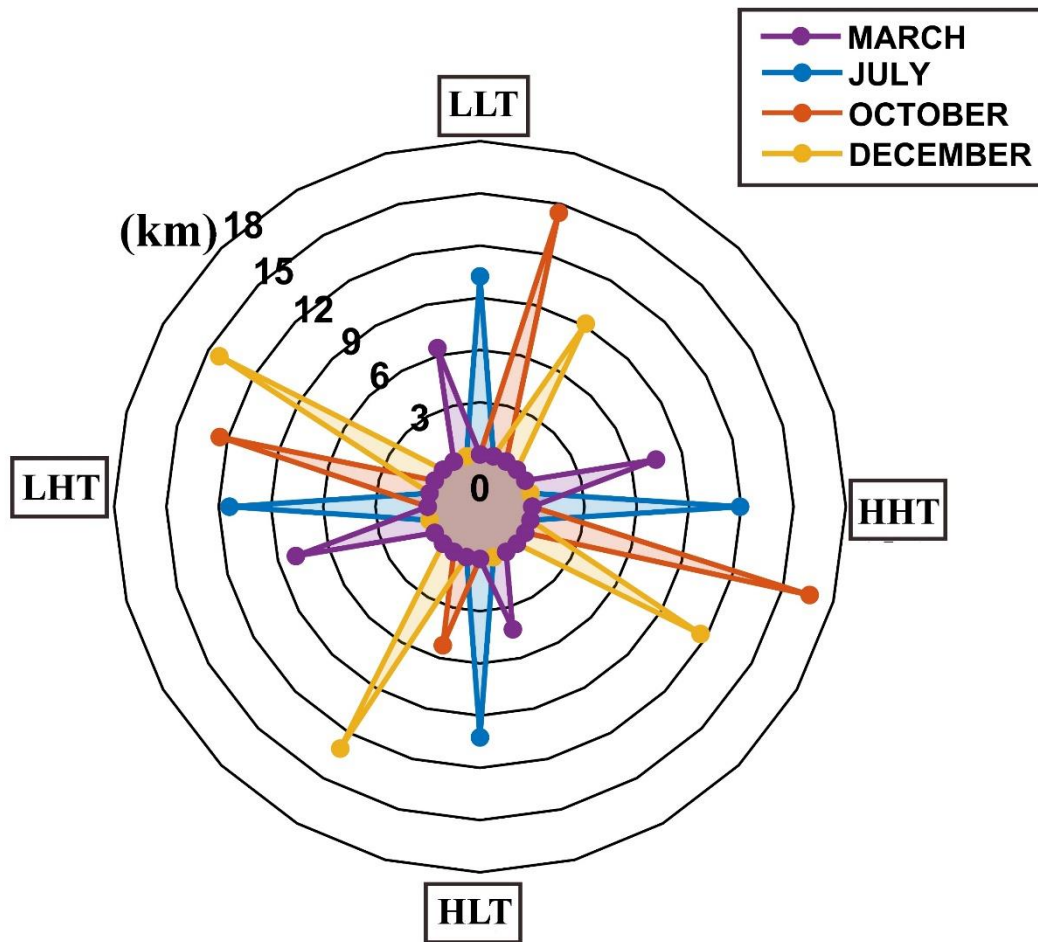


Figure 5. Divulge the time-dependent plume front positioning in respect to varying tidal phases and seasonal river efflux. The orientation of the four colours representing each month (season) is rotated for visibility purposes.

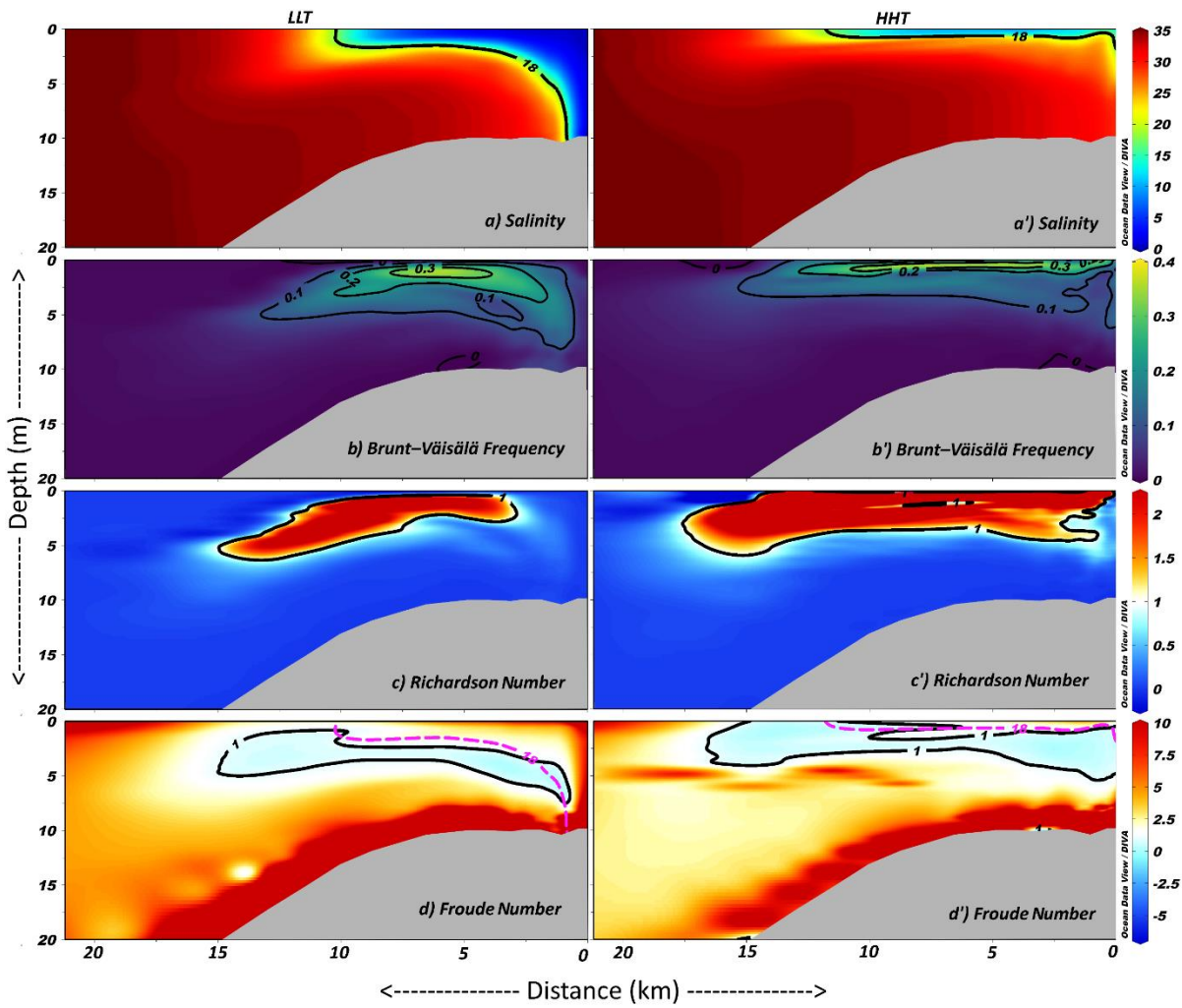


Figure 6. The horizontal and vertical extension of the front and variations in N , R_d and F in the SM during LLT and HHT.

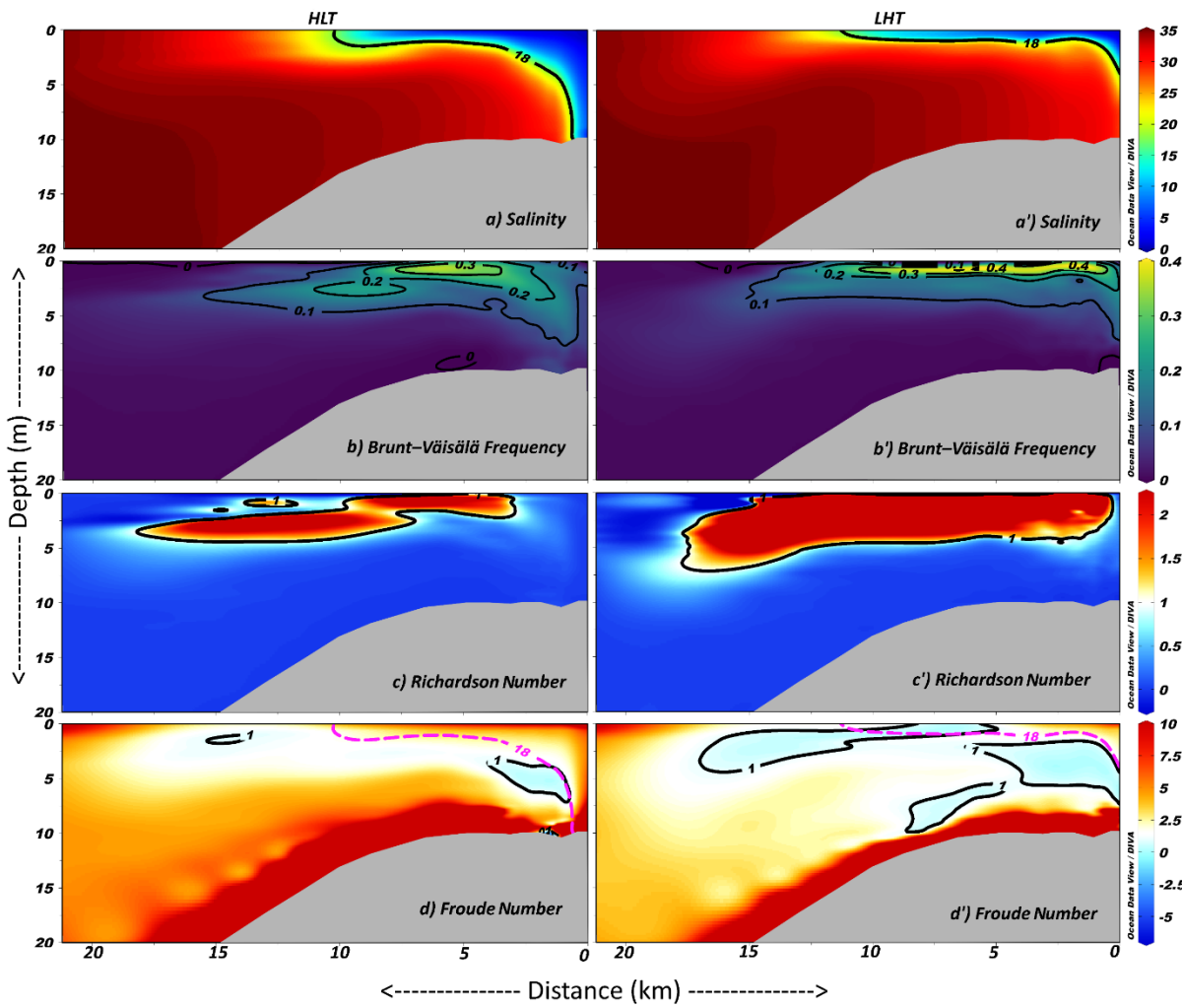


Figure 7. The horizontal and vertical extension of the front and variations in N , R_d and F in the SM during HLT and LHT.

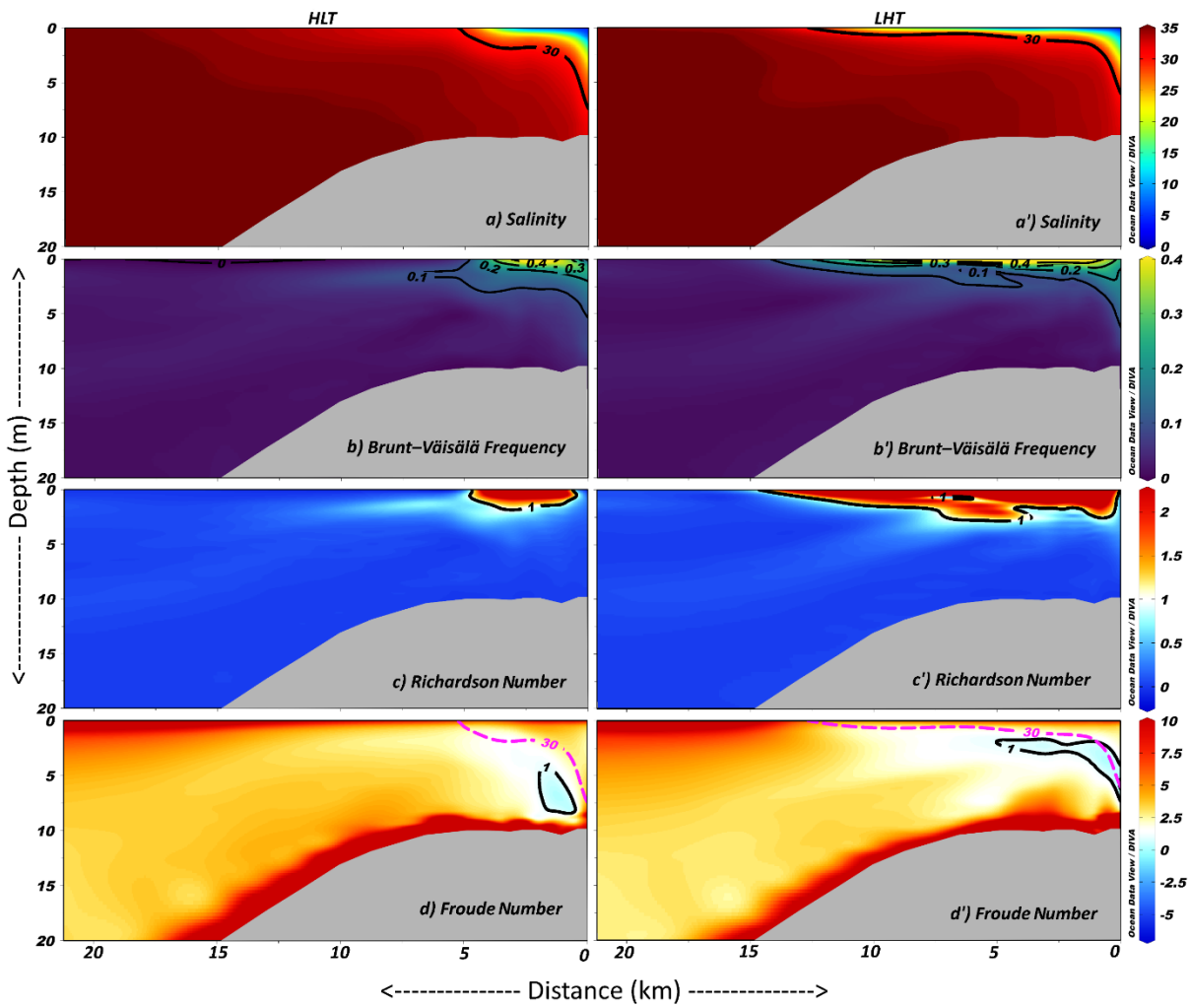


Figure 8. The horizontal and vertical extension of the front and variations in N , R_d and F in the FIM during HLT and LHT.

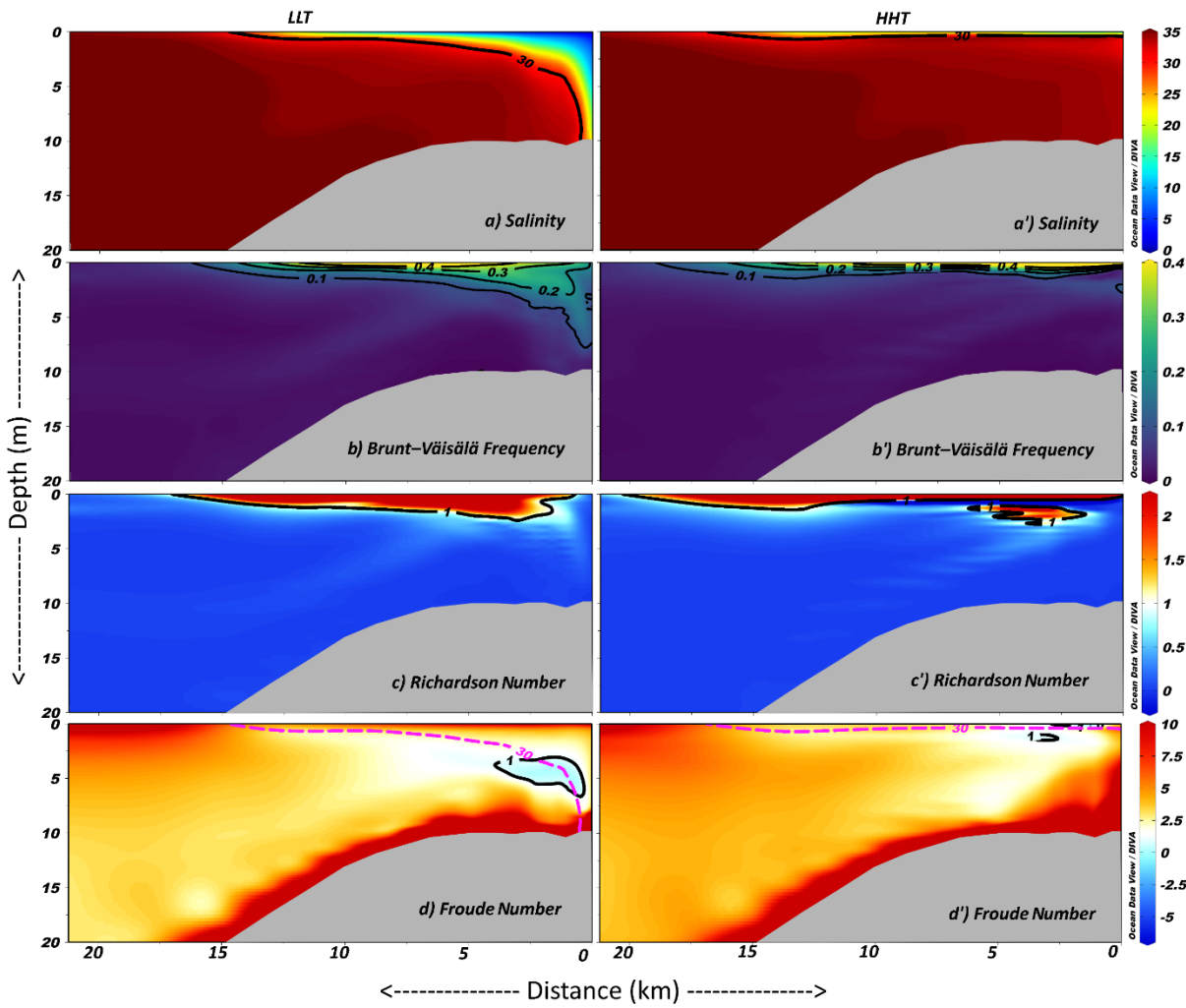


Figure 9. The horizontal and vertical extension of the front and variations in N , R_d and F in the FIM during LLT and HHT.

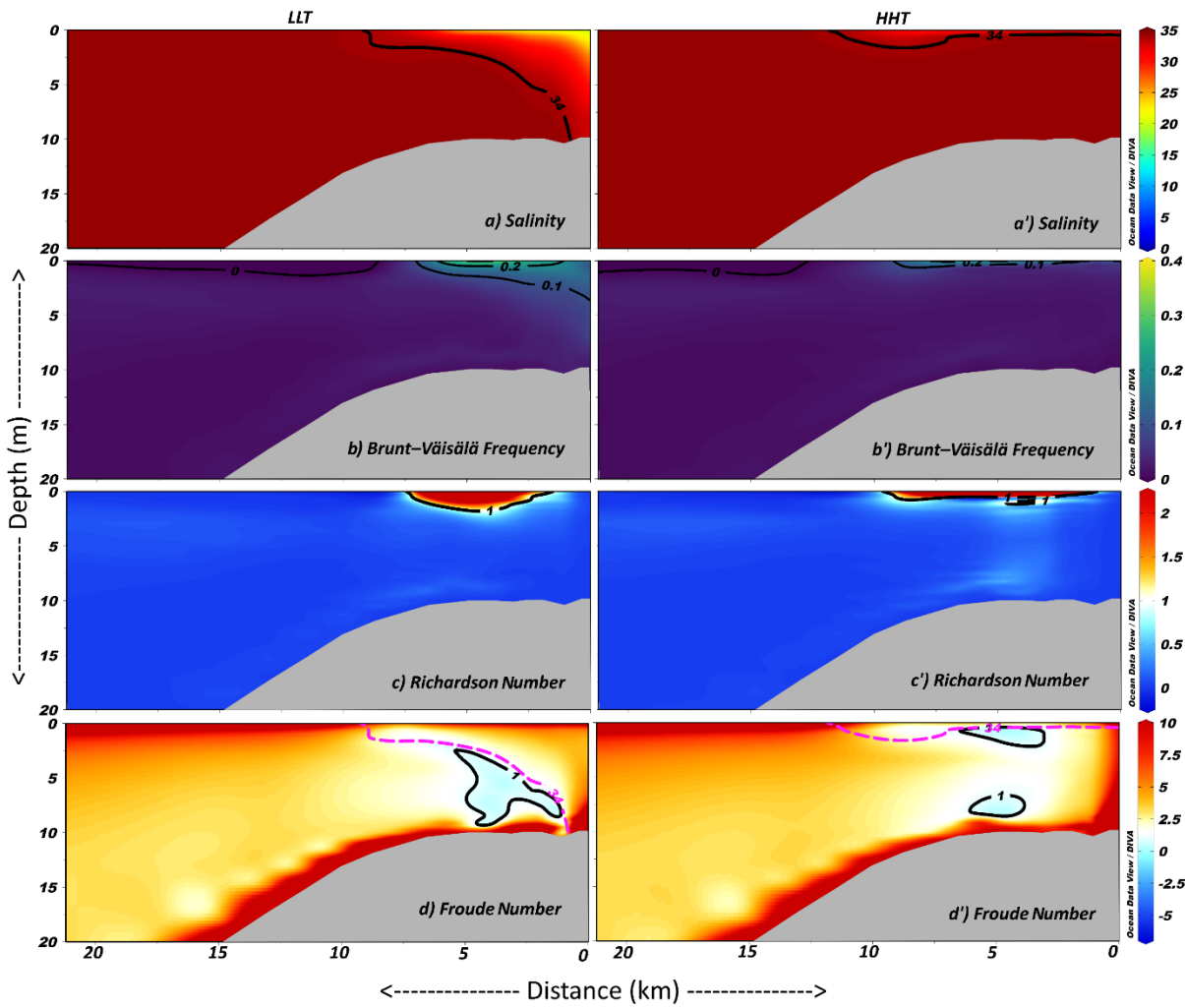


Figure 10. The horizontal and vertical extension of the front and variations in N , R_d and F in the WM during LLT and HHT.

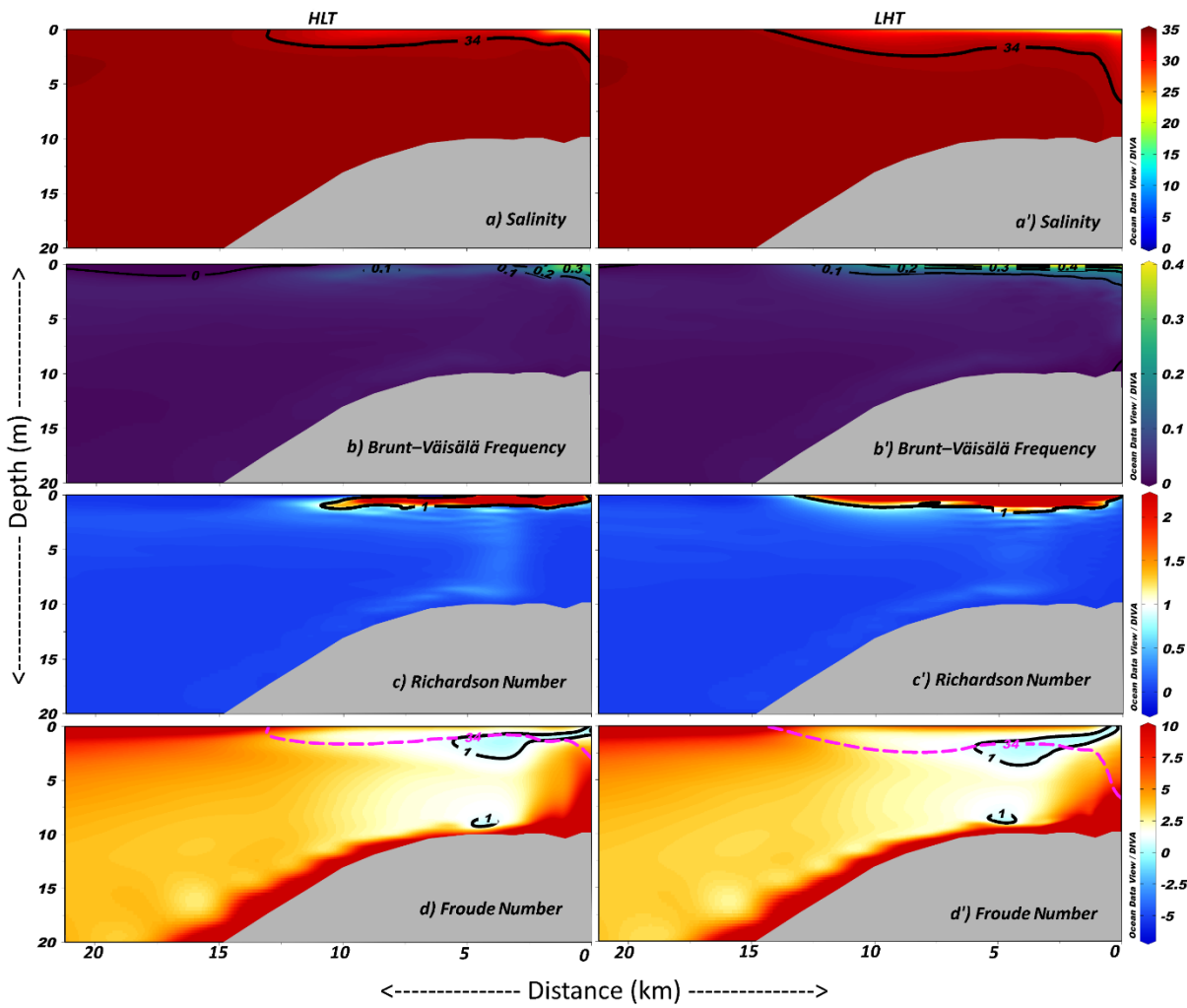


Figure 11. The horizontal and vertical extension of the front and variations in N , R_d and F in the WM during HLT and LHT.

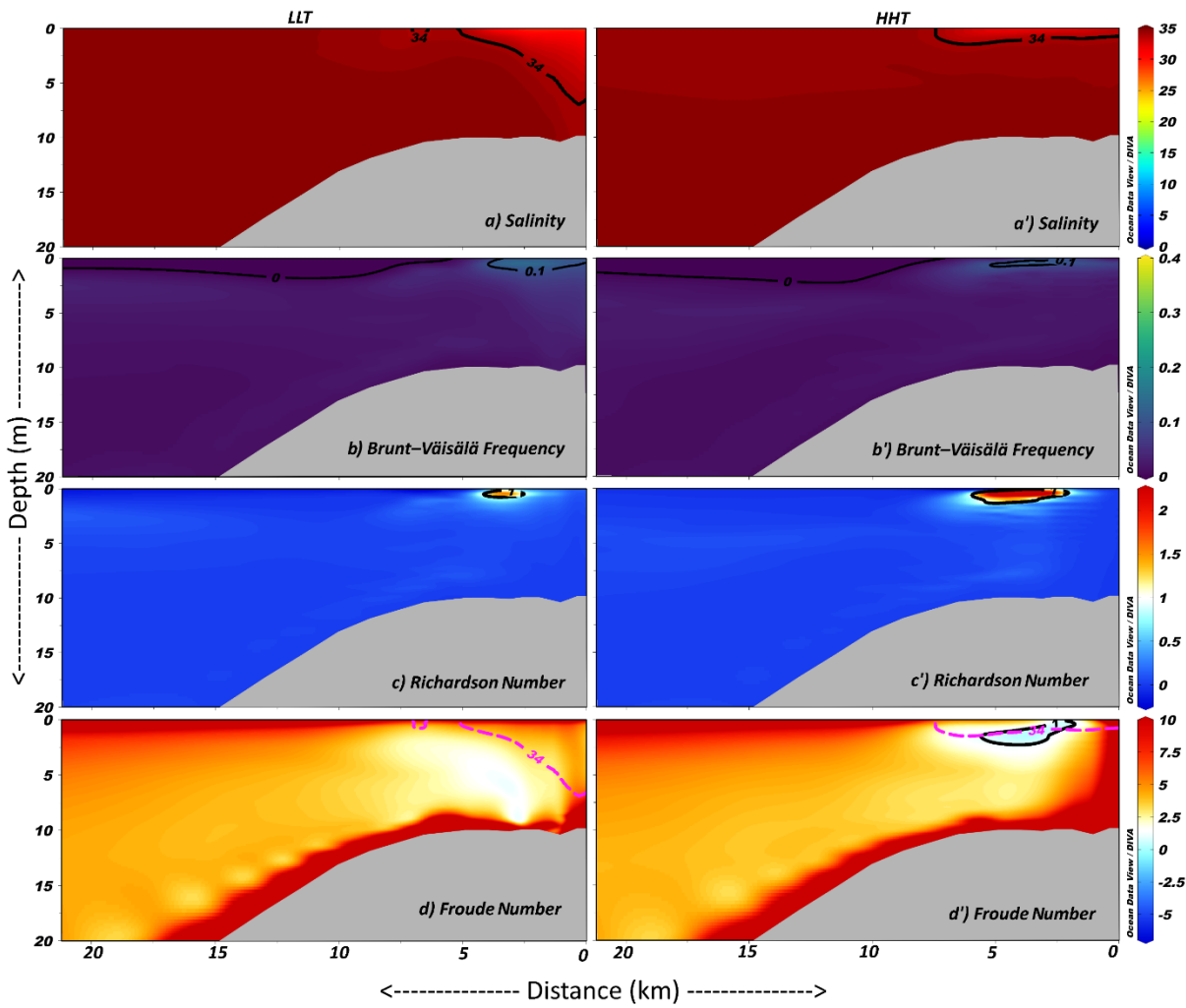


Figure 12. The horizontal and vertical extension of the front and variations in N , R_d and F in the SIM during LLT and HHT.

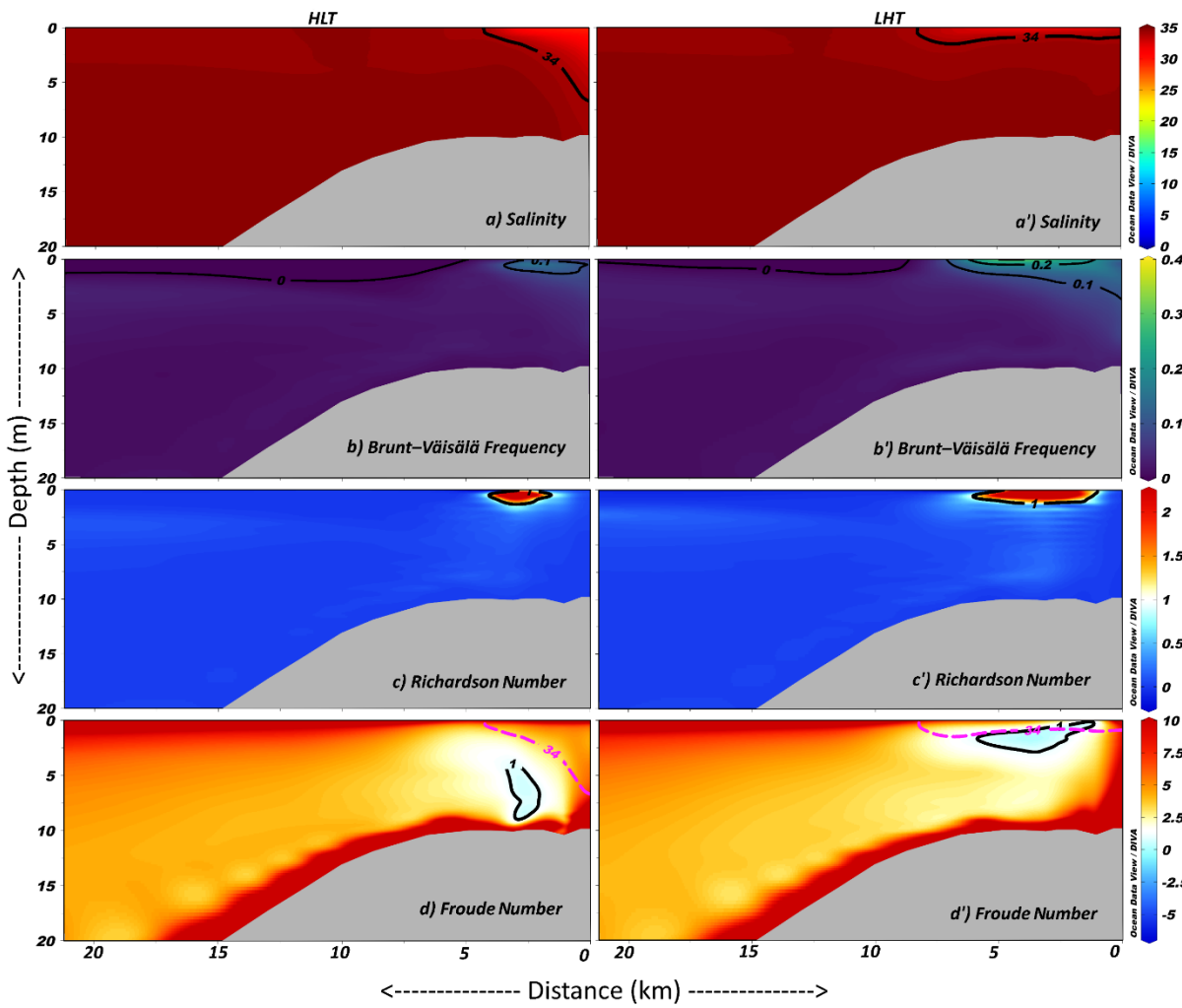


Figure 13. The horizontal and vertical extension of the front and variations in N , R_d and F in the SIM during HLT and LHT.

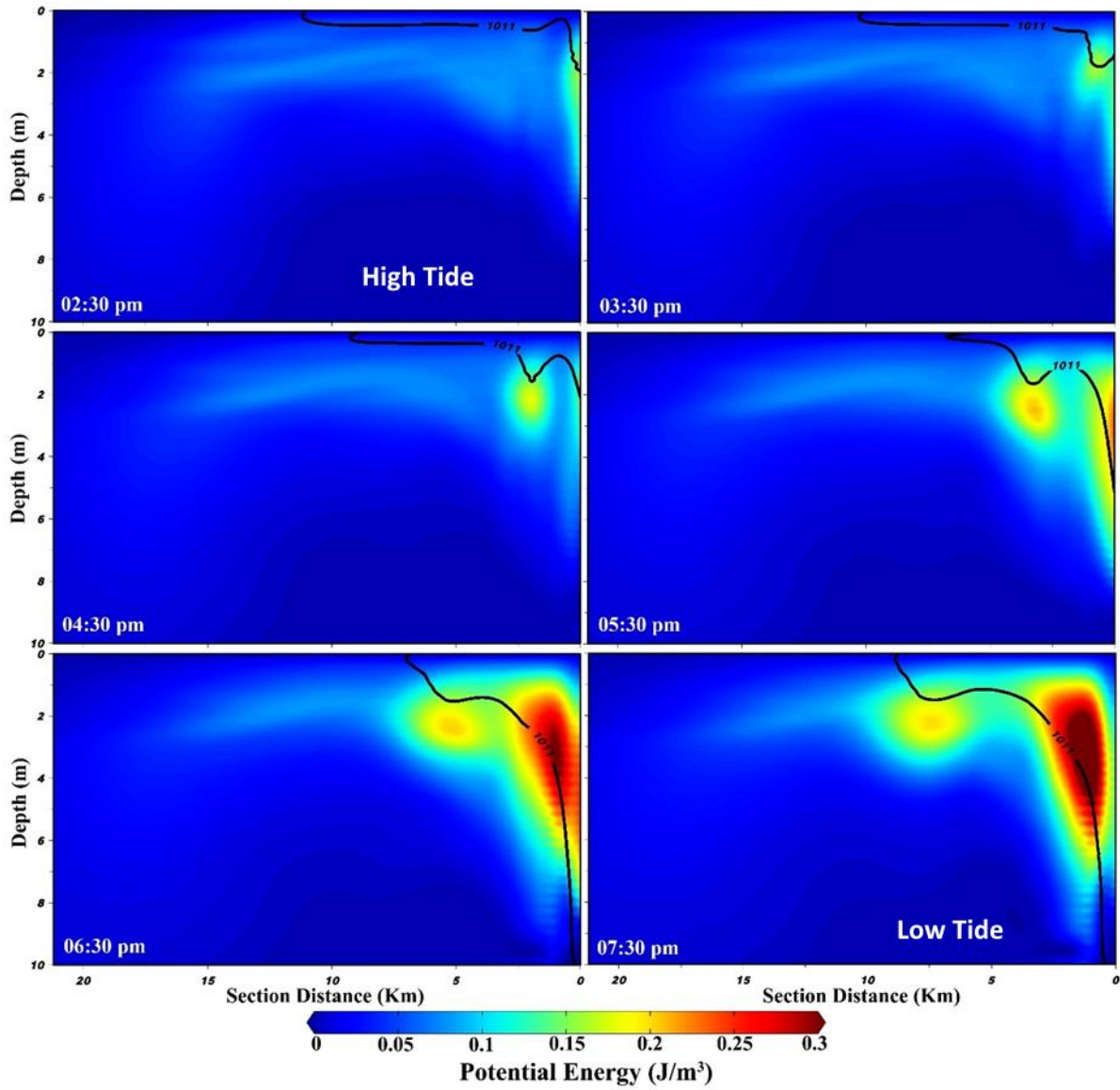


Figure 14. The high potential energy near the Fort Kochi inlet during the high tide to low tide transitional phase. During this phase, the release of potential energy generates a hydraulic jump near the inlet and propagates offshore as an internal wave.

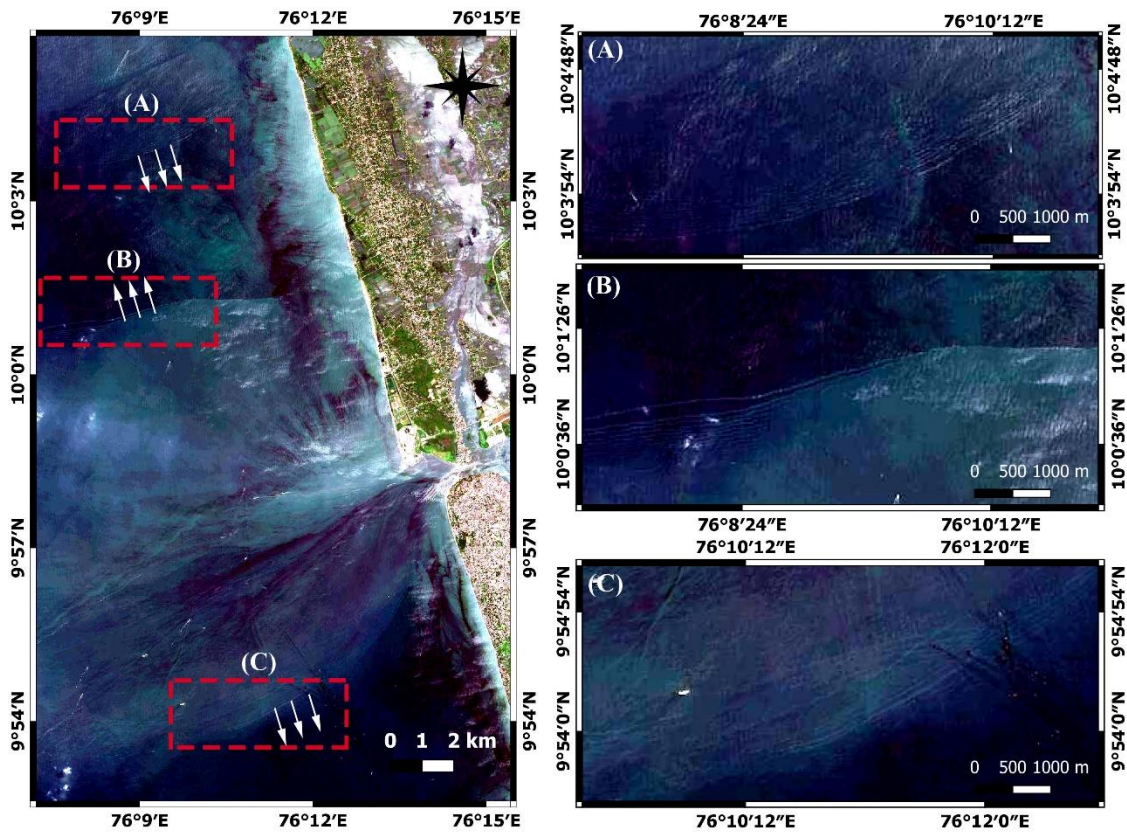


Figure 15. Plume generated internal waves obtained from MAXAR technologies satellite imagery (date: 30/08/2015). Radially outward propagating internal waves can be seen on the left panel, while the right panel shows the more enhanced small scale wave packets in the off Kochi region.